Highlights

Temperature robustness in *Arabidopsis* circadian clock models is facilitated by repressive interactions, autoregulation, and three-node feedbacks

Paula Avello,Seth J. Davis,Jonathan W. Pitchford.

- Temperature dependence is incorporated in a range of circadian clock models

- Key network features allowing temperature compensation are identified

- These features are tested via a set of simple randomly parameterised networks

Temperature robustness in *Arabidopsis* circadian clock models is facilitated by repressive interactions, autoregulation, and three-node feedbacks

Paula Avello[a,*], Seth J. Davis[b,c] and Jonathan W. Pitchford.[a,b]

[a]*Department of Mathematics, University of York, Heslington, York, YO10 5DD, United Kingdom*
[b]*Department of Biology, University of York, Heslington, York, YO10 5DD, United Kingdom*
[c]*Key Laboratory of Plant Stress Biology, School of Life Sciences, Henan University, Kaifeng 475004, China*

ABSTRACT

The biological interactions underpinning the *Arabidopsis* circadian clock have been systematically uncovered and explored by biological experiments and mathematical models. This is captured by a series of published ordinary differential equation (ODE) models, which describe plant clock dynamics in response to light/dark conditions. However, understanding the role of temperature in resetting the clock (entrainment) and the mechanisms by which circadian rhythms maintain a near-24 h period over a range of temperatures (temperature compensation) is still unclear. Understanding entrainment and temperature compensation may elucidate the principles governing the structure of the circadian clock network. Here we explore the design principles of the *Arabidopsis* clock and its responses to changes in temperature. We analyse published clock models of *Arabidopsis*, spanning a range of complexity, and incorporate temperature-dependent dynamics into the parameters of translation rates in these models, to discern which regulatory patterns may best explain clock function and temperature compensation. We additionally construct three minimal clock models and explore what key features govern their rhythmicity and temperature robustness via a series of random parameterisations. Results show that the highly repressive interactions between the components of the plant clock, together with autoregulation patterns and three-node feedback loops, are associated with circadian function of the clock in general, and enhance its robustness to temperature variation in particular. However, because the networks governing clock function vary with time due to light and temperature conditions, we emphasise the importance of studying plant clock functionality in its entirety rather than as a set of discrete regulation patterns.

1. Introduction

Circadian rhythms are the result of positive and negative feedbacks in a network of transcription factors, which regulate the mRNA and protein levels. These complex systems have been modelled in diverse organisms [1, 2, 3] in order to understand the crucial factors driving the circadian oscillations, and in some cases to determine whether clock network structure can determine functionality [4, 5].

Empirically-driven mathematical modelling of the plant *Arabidopsis* had its genesis in the ODE model presented by [6] in 2005, which characterised the interaction between two clock genes and their associated proteins. Since then, several ODE-based models have been built which reflect the increasing complexity of the clock as new biological discoveries arise [6, 7, 8, 9, 10, 11, 12, 13]. Throughout this process, mathematical models have been useful tools to help generate and test hypotheses about the underlying structure of the plant system and to understand its dynamics [14].

The mathematical models proposed to date typically seek to characterise the time evolution of both mRNA and protein levels within plant cells [6, 7, 8, 9, 10, 11, 12, 13] by describing the production and degradation rates of both gene products. A combination of first-order interactions and Hill functions are commonly used to characterise the interactions

within the system [6, 7, 8, 9, 10, 11, 12, 13]. The models are usually parametrized by fitting to experimental observations in a qualitative fashion, principally by matching circadian period, amplitude and phase of gene expression. However, details of the clock mechanism differ between the models, as do the details of the statistical parameter fitting, leading some models to appear to offer a better quantitative fit than others.

Mathematical models for *Arabidopsis* have focused mainly on characterising the plant clock in response to light. Temperature, however, has received less attention and yet its characterization in the plant model system is of increasing importance in the context of global climate change [15]. Experimental evidence has shown that under constant light conditions, and at a constant temperature, circadian rhythms display a relatively invariant period over a large range of temperatures [16, 17]. This is known as temperature compensation. Oscillations with a Q_{10} of period in the range 0.8-1.2 are considered to manifest this feature of compensation [18]. An explanation of this distinctive characteristic of circadian rhythms is based on the hypothesis that there is a resulting balance of network reactions having opposite behaviours [19, 20]. Alternatively, temperature compensation has been explained by the hypothesis that independent molecular mechanisms have evolved in order to establish compensation [18].

In *Arabidopsis*, several clock components have been identified as playing a key role in temperature compensation [16,

17]. However, it is not clear which interactions within the circadian plant network might explain the dynamics of temperature compensation. In biological networks, attempts have been made to explain oscillatory dynamics by analysing the feedback and feedforward loops that form these networks [21, 22]. A feedback loop is defined as positive if the number of negative interactions within the loop is even, or negative if this number is odd, and their basic functionalities can facilitate bistability and promote sustained oscillations, respectively [22]. Feedback loops play different roles within a network, and have been classified broadly with regards to their shape (Figure 1) and functionality [22]. The feedforward loop is a three-component circuit of interactions with edges having inhibitory or activator roles. This circuit is formed by a component that regulates directly and indirectly (through the other component) a target component. Thus, a total of eight possible classes of feedforward loops can be defined (Figure 2). For a description of their dynamical functions, see [23].
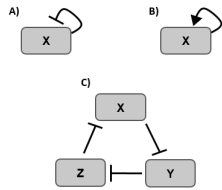

Figure 1: Examples of feedback loops. X, Y, and Z depict genes in a transcription network. Edges in the diagrams are interactions representing how a transcription factor affect the transcription rate of a gene. These interactions may be positive (arrow) or negative (blocked arrow). A) Negative autoregulation. B) Positive autoregulation. C) Three-node feedback loop, also called the *repressilator*.

Feedback and feedforward substructures within biological networks are examples of regulation patterns in real networks which occur more frequently than would be expected in random networks with the same number of nodes and edges [24]. In systems biology, these "regulation patterns" would be described as "network motifs" [25]. We use the former wording in this study, to avoid ambiguity.

The underlying principle is that, if the regulation pattern has been retained over evolutionary time, then it is likely to confer a fitness advantage to the organism [25]. These classes of structures were first detected for the *E.coli* transcription network [26], and from then the interest turned on the detection of their dynamical functions in different organisms and different biological networks [27]. In *Arabidopsis*, regulation pattern analysis carried out under simulated constant light conditions has recently helped to explain the dynamics observed in certain clock mutants [28].

In this work, we analysed the structures of a range of plant clock models proposed over the past 15 years, and added temperature dependence in order to gain insights into thermal robustness of circadian oscillations. We centred our analysis on the transcription regulatory interactions. We asked whether regulation patterns commonly found in other tran-
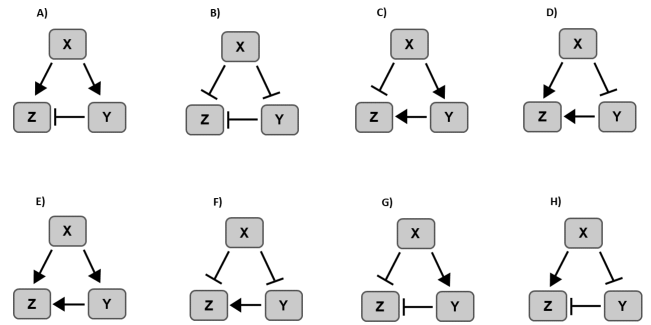
Figure 2: The eight classes of feedforward loops. Feedforward loops are classified based on their *coherent* or *incoherent* effect of a gene X on its target Z. For example, in figure A) X directly activates Z and indirectly represses it as X promotes Y, which is a repressor of Z. This circuit is called *Incoherent type 1*. In contrast, F) shows a gene X repressing its target Z and *coherently* X represses Y, which has an activator effect on Z. F) is termed as *Coherent type 2*. The top row shows the four types of incoherent feedforward loops (from A to D, *Incoherent type 1*, *Incoherent type 2*, *Incoherent type 3* and *Incoherent type 4*, respectively). The bottom row shows the four types of coherent feedforward loops (from E to H, *Coherent type 1*, *Coherent type 2*, *Coherent type 3* and *Coherent type 4*, respectively).

scription networks are involved in temperature-dependent mechanisms in the plant circadian system. To gain a better understanding of the key patterns driving clock function and its robustness to temperature variation, we also performed a large-scale simulation study based on random parameterisations of three simplified models, following [28]. Taken together, our results support the idea that the highly repressive role of transcription factors in the plant clock contributes to its robustness to temperature changes. Our results also show that a simple pattern-based analysis is insufficient to describe dynamics induced by light and temperature; rather, such networks should be analysed as a whole, and as dynamic rather than static networks.

2. Methods

A total of eight ODE-based models of different complexity are analysed, referred to as: L2005a [6], L2005b [7], L2006 [8], P2010 [9], P2012 [10], P2013 [11], F2014 [12], and DC2016 [13]. Because our goal is to describe these models in terms of their structure rather than to focus on each model's biochemical details, we present them as transcription networks and refer the reader to the original papers for a complete description. Although these models show a general pattern of increasing complexity over time, they all derive from a "bottom up" approach to modelling, and may not necessarily capture the full complexity of the actual interactions in the clock. Nevertheless, a structural analysis across these models can lead to useful insight and testable conclusions.

Figure 3 depicts the clock structures of the models. Note

that these networks are derived by considering the mathematical equations governing the dynamics in each case, and that this does not necessarily correspond to the network diagrams published in the original papers, which were in some cases simplified. Figure 3 allows one to visualize the increase in mathematical complexity of the models as new empirical discoveries have been incorporated. Their relative complexity also serves to highlight the difficulty of elucidating the dynamics of the inner transcriptional machinery of the plant oscillator. The interactions are also presented as matrices, which we call *transcription matrices*, see Supplementary Material. The rows in each matrix display the outgoing interactions from transcription factors in the networks, while columns represent the ingoing effect on the transcription rates of the components of the network; the plus and minus signs mean activation and inhibition, respectively. CL again represents *CCA1* and *LHY* when they are modelled as a single variable, and E34L represents *ELF3*, *ELF4* and *LUX* grouped as the evening complex, consistently with the block effect allocated in the models.

Each edge in each network is modelled by a Hill function, which characterises the inhibitor or activator effect of a transcription factor on the rate of production of mRNA. The Hill function is defined by [25],

$$Y = \frac{\beta}{1 + \left(\frac{X}{K}\right)^n},\tag{1}$$

for a repressor, and by

$$Y = \frac{\beta X^n}{K^n + X^n},\tag{2}$$

for an activator, where Y is the rate of production of mRNA, β is the maximal production rate, X is the inhibitor or activator concentration, K is the inhibition or activation coefficient, and n is the Hill coefficient. In other words, each edge in the network is governed by at least three parameters: the repression (or activation) coefficient, the Hill coefficient and a rate constant of transcription. In cases when the transcription of a gene is regulated by a light transient induction effect via interaction with a protein P, a rate constant is also considered to mediate light input.

2.1. Structural description of the plant transcription network

We have carried out a statistical analysis to describe the network structures within the mathematical models for the *Arabidopsis* circadian clock: L2005a [6], L2005b [7], L2006 [8], P2010 [9], P2012 [10], P2013 [11], F2014 [12], and DC2016 [13]. This analysis consists of computing network statistics (number of components, number of edges, density, the average clustering coefficient, and proportion of negative interactions), and then applying a probabilistic approach to quantify the frequency of regulation patterns. In particular, we tested the prevalence of autoregulation, feedforward and

three-component feedback loops by comparing their occurrences in the hypothesised circadian networks against their occurrences in random networks of the same size, following the methodology of [25].

The average number of autoregulation (N_{auto}), feedforward (N_{FFL}), and three-component feedback (N_{Fback}) loops in random networks can be determined by

$$N_{auto} = \frac{E}{N},\tag{3}$$

$$N_{FFL} = \lambda^3 N^{n-e},\tag{4}$$

$$N_{Fback} = \frac{1}{3}\lambda^3 N^{n-e},\tag{5}$$

where $\lambda = \frac{E}{N}$ is the *mean connectivity*, N and E are the numbers of nodes and edges in the network, respectively, and n and e the number of nodes and edges of the particular pattern under consideration (i.e. n=e=3). Note that the average number of autoregulation loops is simply the *mean connectivity*, which can be obtained by characterising the number of autoregulation patterns by a binomial distribution (as we want a determined number of edges out of the total E to be self-loops) with parameters E and p, where p, the probability of having a self-edge, is equal to $1/N$. Therefore, the expected number of autoregulation loops is $E \times 1/N$. For mathematical details of equations 4 and 5 along with equation 3 see [25].

The standard deviations (SD) of these estimations can be calculated by the square root of the equations 3, 4 and 5, and a Z score is used to quantify the significance of the occurrences of these subgraphs. The Z score tells us how many standard deviations the number of the subgraphs observed in the network models exceeds the number expected in random networks, and is calculated as,

$$Z = \frac{\begin{array}{c}\text{number observed} \\ \text{in a network model}\end{array} - \begin{array}{c}\text{expected number} \\ \text{in random networks}\end{array}}{\begin{array}{c}\text{standard deviation} \\ \text{in random networks}\end{array}}.$$

(Note that, with the exception of the [13] model where *ELF4* and *LUX* are merged into a single variable, statistical calculations in models including the evening complex were performed taking *ELF4*, *ELF3* and *LUX* into account as individual components.)

2.2. Temperature dependence

Following the methodology of [15], we incorporated temperature dependence into the models by allowing translation rates to vary with temperature. Arrhenius equations were applied to the relevant parameters (see Table S1, Supplementary Material) by using a reference temperature of 22°C in all models in order to match their published parameter values corresponding to this temperature. With the aim to assess
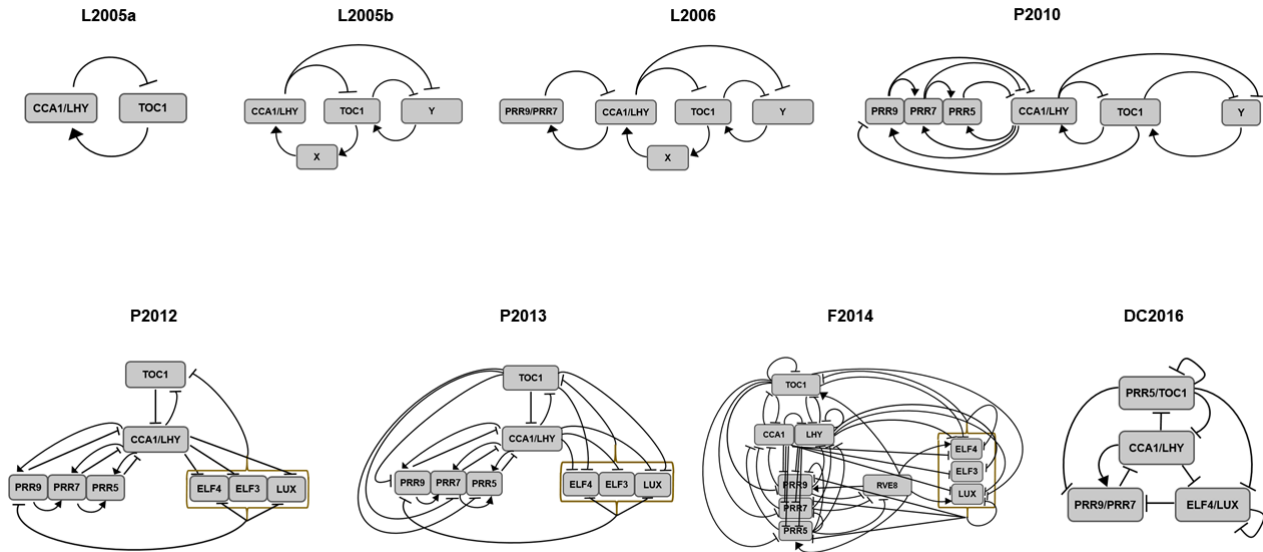
Figure 3: Developments in ODE-based models for the *Arabidopsis* circadian clock. Transcription networks are illustrated for eight models for the plant clock. The plant oscillator was first modelled as a simple negative feedback. As more clock components were discovered, three-node circuits were incorporated, and the wiring of the plant network became more complicated. The most recent clock model structures incorporate autoregulation patterns, and have mainly repressive interactions. The models are abbreviated as follows: L2005a [6], L2005b [7], L2006 [8], P2010 [9], P2012 [10], P2013 [11], F2014 [12], and DC2016 [13].

whether the models were temperature compensated, an activation energy value of 50 kJ mol^{-1} was used for each rate. This value allows us to model a Q_{10} of rate equal to 2, which is a standard value accepted for most biological reactions [18]. Simulations were carried out according to the experimental protocols of [16] and [17]. A model was considered compensated if its overall Q_{10} of period was in the range between 0.8 and 1.2 [18]. To test whether these conclusions were reliable, we also ran simulations incorporating variability in the influence of temperature by randomly choosing each activation energy value independently from a uniform distribution between 40 kJ mol^{-1} and 60 kJ mol^{-1}; this corresponds to values for Q_{10} between 1.8 and 2.3 approximately. Two hundred replications of those random parameterizations were performed for each model, which gave us a reasonable representation of the variability between replicates (see Figure S1 in Supplementary Material). Temperature compensation was assessed in each case.

Note that in [12], the authors modelled the protein production rate as equal to one copy per mRNA for all transcription factors with the exception of *ELF4* and *ELF3* components. This approach differs from that of other models, where protein production is usually characterised by p copies of mRNA that are translated (with the translation rate p not necessarily equal to 1 h^{-1} in most cases). Thus, to incorporate temperature into [12] model, we extended that model by adding parameters p_j, (j representing a component model) in

the terms of protein production rates of the dynamical equations labeled by (5), (7), (10), (12), (15), (20), (30), (45) in [12]; p_1, p_2, p_3, p_4, p_5, p_{30}, p_{31}, and p_{32}, respectively. We fixed the p_j values to be equal to 1 at the temperature reference 22°C in order to preserve the original model and followed to proceed with allowing them to vary with temperature as described previously.

## 2.3. Numerical Investigation of minimal models via random parameterisation

A recent study by [28] provides an interesting alternative approach towards discovering the design principles of the circadian clock by proposing a number of possible clock structures and investigating their emergent properties by a series of random parameterisations. Motivated by this study, and to complement the results emerging from the more complex models L2005a [6], L2005b [7], L2006 [8], P2010 [9], P2012 [10], P2013 [11], F2014 [12], and DC2016 [13], we investigated three simplified clock structures (Figure 4) of four repressor components, which represent *CCA1/LHY*, *PRR9/PRR7*, *PRR5/TOC1* and *ELF4/LUX*, in order to assess changes in the periodicity of the plant clock. These clock structures incorporate the direct repressive effect of *CCA1* and *LHY* on *PRR9* and *PRR7* reformulated recently [29, 30] and also modelled in [28, 12]. As in the analysis of the historical models, parameters of translation rates in these models were allowed to vary with temperature under a simulated continuous light condition (as in [28]) fol-
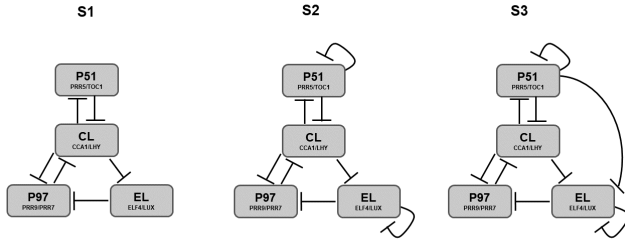
Figure 4: Minimal clock model structures. Structure S1 includes a three-node feedback loop. In S2 autoregulation patterns were added to end up with S3 structure having a feedforward loop. All clock components are characterised to have a repressive role within the network.

lowed by incorporation of temperature dependence in transcription rates for comparison. Because our goal was to analyse structural patterns that may explain temperature compensation, our models are not expected to faithfully reproduce the detailed behaviour of the plant circadian system. Rather, we asked which structures and parameterisations allow these minimal models to show regular oscillatory behaviour and an empirically justifiable phasing of peak expression levels (i.e. the order of the peak mRNA levels of the clock components should agree with that observed in reality, with *CCA1* and *LHY* peaking before *PRR9* and *PRR7*, followed by the peak of *PRR5* and *TOC1* before *ELF4* and *LUX*).

Consistent with the more complex models, the proposed structures are characterised by systems of ODEs for mRNA and protein levels (see Supplementary Material for details). The parameter values were assigned randomly from independently uniformly distributed numbers between 0 and 1. In the same manner, Hill coefficients were assigned from discrete uniform distributions on the range between 2 and 4. The initial conditions of the system were fixed to be equal to 0.1 in all cases. By using a notional unit of time of an hour, the clock was run for 20 days and the first 10 days were not included in the analysis in order to avoid transient effects [13]. Next, we searched for parameter sets reproducing oscillatory behaviour. The period of the system was calculated by measuring the time difference between consecutive troughs. We then selected from those sets the parameter values that showed the correct phase for the peak of the gene expression, and went on to incorporate temperature dependence in the translation rates.

To compare models, hitting rates were calculated [28, 31]. This measure gives us an averaged proportion of the parameter sets that met our selection criteria, with respect to the total number of parameters that were generated at random in the researching scheme. The higher the hitting rate, the more robust the model against parameter combinations.

This proportion is defined by,

$$P = \sqrt[n]{\frac{\text{number of obtained parameter sets}}{\text{number of searched parameter sets}}}, \quad (6)$$

where n is the number of independent parameters.

3. Results

3.1. Description of the hypothesized clock plant structures

Table 1 shows the basic network statistics of the models under consideration. The networks are all much more dense, and more clustered, than the large-scale transcription networks typically observed in systems biology [25]. It should be noted that, as model complexity (number of components) increases, there is no useful trend in the density or clustering coefficient of the networks; the circadian models are all dense well-connected networks. It is also noteworthy that the proportion of negative interactions is much higher in models from 2012, surpassing the number of positive interactions. Table 2 extends this comparison by looking at the prevalence of regulation patterns in comparison to Erdos-Renyi random graphs of the same size and density. It may be noted that the occurrence of three-component feedback loops is more common in models from 2012; Z scores for P2012, P2013 and F2014 showed that they appear more often than would be expected at random as their Z scores represent higher deviation from the mean in random graphs.

Figure 5 summarises the main results concerning temperature compensation and clock behaviour in changing temperatures; when translation rates are allowed to vary with temperature, only the more recent (and more complex) models exhibit temperature compensation and sustained oscillations on the whole temperature range of 12°C - 28°C. The earliest clock models, L2005a, L2005b and L2006 only function within a narrow temperature range; at lower temperatures the rhythms were disrupted. Temperature compensation was not observed in the models L2005a and L2005b, the clock slows down, or speeds up, markedly as temperature increases in these early models before all rhythmic behaviour is lost (L2005a, L2005b and L2006). The more complex P2010 model, compared to L2005a, L2005b and L2006 models, functions across a broader temperature range and at temperatures lower than 18°C displays temperature robustness, but is similarly uncompensated from 18°C. However, the most complex and most recent models P2012, P2013, F2014 and DC2016 all show temperature compensation to a greater or lesser extent. Figures S2 and S3 in Supplementary Material show that this finding is not an artefact of the fixed choice of activation energy in the simulations in Figure 5. When activation energies are allowed to vary between 40 kJmol⁻¹ and 60 kJmol⁻¹ the same patterns emerge; only the models P2012, P2013, F2014 and DC2016 exhibit temperature compensation, but this temperature compensation is robust to variability in activation energy.

Table 1
Network statistics of the *Arabidopsis* circadian models illustrated in Figure 3.

	Global properties				
ODE model	number of components	number of edges	density	clustering coefficient	prop. of neg. interactions
L2005a	2	2	0.50	-	0.50
L2005b	4	6	0.38	0.83	0.50
L2006	5	8	0.32	0.75	0.50
P2010	6	14	0.39	0.73	0.50
P2012	8	17	0.27	0.82	0.71
P2013	8	22	0.34	0.87	0.77
F2014	10	46	0.46	0.92	0.89
DC2016	4	10	0.63	1	0.90

Table 2
Comparison of the regulation patterns found in a range of circadian models, with those expected at random for graphs with the same size and density (mean $\pm$ 1$\times$SD). Z scores are shown in cases when expected values are exceeded.

|	Regulation patterns					
ODE model	autoregulation	expected autoregulation	feedforward	expected feedforward	feedback	expected feedback
L2005a	0	1 $\pm$ 1	-	-	-	-
L2005b	0	1.5 $\pm$ 1.2	2	3.4 $\pm$ 1.8	1	1.1 $\pm$ 1.1
L2006	0	1.6 $\pm$ 1.3	2	4.1 $\pm$ 2.0	1	1.4 $\pm$ 1.2
P2010	0	2.3 $\pm$ 1.5	10	12.7 $\pm$ 3.6	4	4.2 $\pm$ 2.1
P2012	2	2.1 $\pm$ 1.5	13 (Z=1.1)	9.6 $\pm$ 3.1	6 (Z=1.6)	3.2 $\pm$ 1.8
P2013	2	2.8 $\pm$ 1.7	23 (Z=0.5)	20.8 $\pm$ 4.6	11 (Z=1.5)	6.9 $\pm$ 2.6
F2014	4	4.6 $\pm$ 2.1	115 (Z=1.8)	97.3 $\pm$ 9.9	50 (Z=3.1)	32.4 $\pm$ 5.7
DC2016	2	2.5 $\pm$ 1.6	7	15.6 $\pm$ 4.0	2	5.2 $\pm$ 2.3

Although the Q_{10} of period observed in the most recent models suggests that complexity is helpful in facilitating temperature compensation, it is not possible to attribute this phenomenon to any regulation pattern in particular. For example, because clock models presenting autoregulation patterns display robustness against variation in translation rates due to temperature changes, it might be tempting to explain this robustness as a result of autoregulation patterns. However, this is not the case as shown in Figure S4, where outputs are presented for both P2012 and DC2016 models in the absence of their autoregulation loops; temperature compensation is maintained. Indeed, repeating investigations similar to these but with changes to feedback and feedforward loops revealed no clear patterns (see Figures S5 and S6 in Supplementary Material).

Interestingly, when temperature compensation was tested under constant dark condition in DC2016 model (see Figure S7 in Supplementary Material), compensation was still observed; however, the Q_{10} of period was reduced from 0.97 to 0.94. Note that *ELF4/LUX* autoregulation coupled with three-node feedback loops are not present in the DC2016 model under dark conditions (see Figure 1 in [15]). These results suggest that autoregulation combines with three-node

feedback loops to form a highly inhibiting transcription network which contributes to temperature compensation. These ideas are tested in the following section.

3.2. Minimal models via random parameterisation

We defined three minimal structures for numerical investigation (S1, S2 and S3 in Figure 4) in order to test whether the inclusion of certain well-defined regulatory patterns may facilitate temperature compensation in simple models. Figure 6 depicts the main results when the behaviours of these models are compared, using random parameterisations and the criteria for periodicity and compensation as explained in Methods. Surprisingly, across the range of random parameterisations, we found no important differences between the models S1, S2 and S3 in terms of their ability to produce sustained oscillations with the correct ordering of peaks in gene expression (Figure 6A). Moreover, all structures presented high hitting rates, indicating that a large percentage of parameter sets met our criteria of oscillatory behaviour and proper order of peak mRNA levels. However, we did find differences when temperature dependence was incorporated into these models. Figure 6B shows that the incorporation of autoregulation patterns improves the robustness of the system across an extended temperature range; the model S2 showed a much higher proportion of oscillating parame-
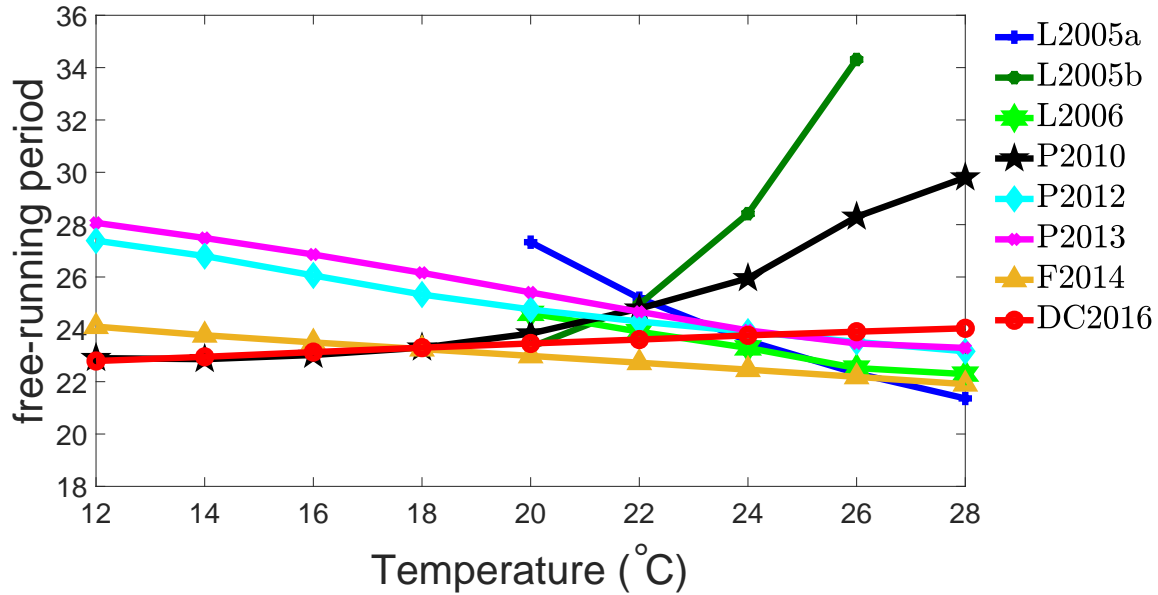
Figure 5: The models P2012, P2013, F2014 and DC2016 exhibit temperature compensation. Simulations were carried out following experimental protocols of [16] and [17]. The earliest clock models, L2005a, L2005b and L2006 allow incorporation of temperature into the plant clock, but only function within a reduced temperature range; at temperatures lower than 20°C the clock is disrupted. Temperature compensation is not observed in the models L2005a and L2005b, and nor in L2006 and P2010 for the whole temperature range under consideration; the clock either slows down (L2005b, P2010) or speeds up (L2005a) markedly as temperature increases in these early models. In contrast, the models P2012, P2013, F2014 and DC2016 show temperature compensation effectively across the entire temperature range of 12°C - 28°C, with Q_{10} values on this range equal to 1.11, 1.12, 1.06 and 0.97, respectively.

ter sets that tolerated temperatures between 12°C and 28°C compared to the model S1. Note that the models S2 and S3 showed similar results, which suggests that feedforward loop is not required to extend the tolerable temperature range, but that three-node feedback and autoregulation patterns are required together to allow the system to oscillate in extended temperature ranges.

Figure 6C shows the distribution of the Q_{10} of period for each model under random parameterisation. Although model S1 displays robustness against temperature changes with 62% of its parameter sets allowing the system to achieve temperature compensation (Q_{10} lying within the range 0.8-1.2), it is evident that adding autoregulation patterns significantly improved this robustness. Outcomes of the model S2 showed that 83% of the parameter sets presented Q_{10} values in the range for compensation. Moreover, the Q_{10} distribution shifted to locating closer to perfect compensation (i.e. $Q_{10} = 1$); the median of the distribution shifted from a Q_{10}=0.83 in model S1 to a Q_{10}=0.90 in model S2. It is also possible to observe a reduction in the dispersion of the distribution; the range of the Q_{10} values is reduced by 14%. However, this improvement was affected when feedforward loop was incorporated into the system. In model S3, the percentage of parameter sets resulting in Q_{10} values in the range for compensation dropped to 76% and its distribution was more spread out, the range of the modelled outcomes increased by 43% compared to model S2, and this increased variability is mainly caused by values below the median.

These results were challenged by including temperature dependence in the transcription rates of our models. As shown in Figure 6D-E, similar results were found. Adding autoregulation patterns improved considerably the robustness of the clock to cope with temperature variation; the proportion of sets of random parameter combinations allowing the clock to oscillate between 12°C and 28°C was doubled (Figure 6D) and the great majority of these parameter sets permitted the system to be temperature compensated with Q_{10} values closer to perfect compensation (Figure 6E). It was also observed that adding a feedforward loop did not make a significant difference; although on this occasion the model was rhythmic between 12°C and 28°C for a slightly higher proportion of sets, there was no improvement in terms of Q_{10} values. In addition, we tested the clock behaviour by making both translation and transcription rates temperature dependent, and the results also supported a clock structure with autoregulation and three-node feedback loops (Figure 6F-G).

Note that when we compared between conditions rather than between model structures, all models behaved more robustly under temperature-dependent translation rates. For example, a 14.7% out of the selected parameters sets in model S1 for translation-dependent rates produced sustained oscillations on the temperature range of 12°C - 28°C (Table S3), whereas a reduced percentage (9.6 %) was found for transcription rates (Table S4). Moreover, when both rates were
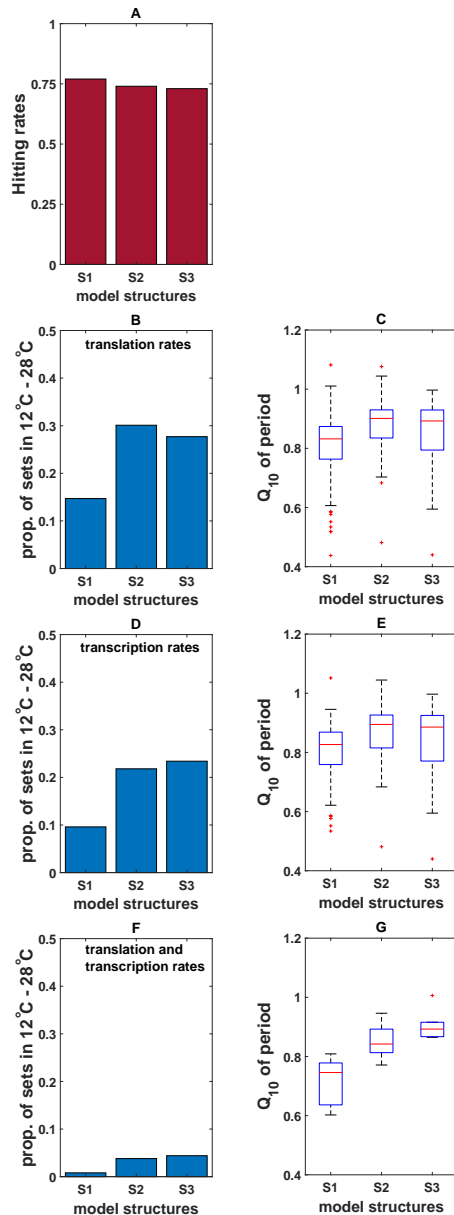
Figure 6: Autoregulation together with three-node feedback structure improves the robustness of the system against temperature changes. Results from random parameterisations of models S1, S2 and S3 in Figure 4. (A) Normalized proportion of parameter sets that showed sustained oscillations and correct order of peak gene expression. (B, D, F) Proportion of parameter sets that allowed the system to oscillate across a 12°C - 28°C temperature range with respect to the number of sets obtained after searching (see Tables S3 to S5 in Supplementary Material for absolute frequencies). (C, E, G) Distribution of the modelled outputs of the parameter sets selected to show oscillatory behaviour in the range 12°C - 28°C.

allowed to vary with temperature, the number of sets that displayed oscillatory behaviour on this range was significantly smaller (Table S5), making their resulting distribution of Q_{10} values less reliable.

4. Discussion and Conclusions

Particular subgraphs in transcription networks have been argued to drive specific tasks and to favour particular behaviours in biochemical systems [25]. The interest in the study of these graph structures is founded on the hypothesis that they are the result of evolutionary selection [25]. We studied whether temperature compensation can be explained by the function of specific subgraphs (regulation patterns) in the plant circadian network by exploring the structures in a range of *Arabidopsis* circadian clock models, and by numerical investigation of three minimal models via random parameterisation. We found that temperature compensation cannot be determined as a function of a particular substructure of the currently published models, but it involves a global property of this network, where autoregulation together with three-node feedback loops in a transcription network dominated by negative interactions favour the clock to be robust to temperature variability.

Exploring the range of models for the plant circadian system, we found that only clock models presenting autoregulation patterns displayed robustness against variation in translation rates due to temperature changes. Surprisingly, we also found that this cannot in itself be the cause of robustness to temperature variation; results from modified P2012 and DC2016 models to exclude autoregulation structures showed that these models still exhibit temperature compensation (Figure S4 in Supplementary Material). Similarly, we observed that compensated models have the particular feature of presenting a much higher proportion of negative regulations compared to uncompensated models (Table 1); however, removing the positive interactions or changing them by repressive roles in P2010 model did not change the uncompensated dynamics of this model but instead, the clock function was disrupted and no oscillations were observed (see Figure S8 in Supplementary Material). Additionally, our results (Table 2) suggest that the three-node feedback loop might favor the robustness of the plant clock against temperature changes, as these patterns occur more often in compensated models. This motivates the investigation of three minimal models, to help understand the effect of adding new interaction patterns to the *Arabidopsis* system under thermal variation. The results from these models show that adding autoregulation patterns to a network with a three-node feedback loop improves the temperature tolerance; however, adding a feedforward loop reduces the performance of the oscillator in the face of temperature changes.

We have shown the sufficiency of a clock structure having autoregulation patterns together with a three-node feedback loop for robust temperature compensation. In order to establish the necessity of a clock structure having those regulation patterns, we have taken structure S1 (Figure 4) and have removed the repressor effect of CL on EL so as to withdraw the three-node feedback loop in a structure with no autoregulation patterns. We then parameterised the resulting clock network by random searches and analysed it as described in Method section. From the 500,000 sets of random parameter combinations, only 36 sets showed oscilla-

tory behaviour and none showed the correct phase of peak of the gene expression. Therefore, because this structure does not fulfill our selection criteria (see Method section), which is a basic yardstick to assess a representation of the plant circadian oscillator, it may be reasonable to conclude that a clock structure having autoregulation patterns together with a three-node feedback loop is a condition necessary and sufficient for temperature robustness.

The results from the minimal models rely on random parameterisations, and may therefore be influenced by the necessarily arbitrary range of values from where they were chosen. To test whether the results are limited to parameter values chosen at random from uniformly distributed numbers between 0 and 1, we implemented the proposed minimal models but with parameter values chosen with closer reference to published parameter values. Explicitly, we took the relevant parameter values of DC2016 model and allowed these to vary according to a uniform distribution on the boundaries zero and two-fold their original values, independently for each parameter. (We note, however, that defining a unique correspondence between these minimal models and the parameters in the more complex DC2016 model is impossible.) Similarly to the modelled inputs for Figure 6, Hill coefficients were chosen randomly on the range between 2 and 4, and a total of 500,000 sets of parameter combinations were generated for the analysis. Figure S9 in Supplementary Material shows the modelled outputs of these random parameterisations. The same overall conclusion emerges; autoregulation patterns together with a three-node negative feedback loops in a network dominated by negative interactions favor temperature compensation, which is consistent with the results of the analysis from the historical clock models. There is, however, a notable change in the sensitivity of the proportion of temperature compensated parameter sets; although the ranking of models S1-S3 is unchanged, the differences in the proportions are minimal. A principal components analysis explored these sets of parameter combinations in order to examine whether there were patterns within the successful parametrizations. No clusters emerged either on the basis of the parameter sets that allowed the clock models to oscillate within the temperature range 12°C - 28°C, or when outputs were grouped to distinguish compensated sets.

We have applied ideas from systems biology to an exploratory analysis of the plant circadian clock. We found that autoregulation and feedforward loops are not found more frequently in these proposed *Arabidopsis* networks, compared to random networks. However, three-node feedback loops appear slightly more often in the hypothesised transcription networks for *Arabidopsis* from 2012. Note that only the F2014 model showed a Z score greater than 2, which is usually used as a threshold for statistical significance [24]. We also found that the hypothesised networks are not sparse, but they are dense. In the context of transcription networks, density values less than 0.001 are common, whereas the historical models of circadian networks do not show densities less than 0.27. Out degree distributions are not long tailed, the degree distributions are compact, and there is no clear

pattern to their shapes. These facts are likely to be consequences of the bottom-up modelling paradigm, where new biological detail is added to models as and when empirical evidence allows. We also observed that the hypothesised transcription networks for the plant clock are highly clustered (*i.e.* clustering coefficients much larger than density values), which implies that their average clustering coefficient is larger than those in random graphs. The latter is in agreement with observations of transcription networks of other systems [25], but it has not proved possible to make a theoretical link from this observation to statements about general clock function and temperature robustness.

We assume for simplicity that translation rates vary with temperature, but that rates of transcription and degradation remain constant. We accept that there is evidence of temperature sensitivity in these rates [32]. Previously, we have shown that temperature dependence of translation and transcription rates can facilitate a compensated clock, and that degradation rates can be important in determining the range of compensation; specifically, we observed that in some *Arabidopsis* models degradation rates may drive the failure to compensate [15]. Our simplified approach here is comparable to that used in studies of *Neurospora* [33, 20], which assume small activation energies for the degradation rates of the model, making those practically insensitive to temperature, in comparison with larger values assigned to transcription and translation rates. However, modelling the influence of temperature in the full range of post-transcriptional and/or post-translational processes is still an open question which will merit attention when better empirical data become available.

Although the minimal models studied here necessarily have some limitations, being highly oversimplified systems to represent complex plant dynamics, they provide helpful insights into what design principles of the *Arabidopsis* transcription network have an important role in rhythmicity and temperature robustness. Our observations support that mathematical and graph-theoretic approaches are useful in the analysis of the plant clock as a whole system. The importance of external cues, whether of light, temperature, or both, has the effect of enforcing dynamic networks of interaction on the plant clock, a fact not taken into account in the traditional systems biology theories ([25]), and this is likely to limit the applicability of the theory in general.

With this in mind, it may be useful for future studies of circadian networks to embrace network analysis as applied to social and ecological systems. For example, in behavioral ecology, analyzing social network activity over time gives valuable information about the causes and consequences of animal sociality [34, 35]. Temporal sampling is carried out to collect social data in order to construct an underlying social network, and temporal interactions between animals are then represented by two types of networks: 1) time-ordered networks, where the duration of the interactions is considered, and 2) time-aggregated networks (a simplification of the time-ordered approach), where a sequence of static networks are analysed [36, 37]. It is also worth noting that

the emergent outcomes of simulating ecological dynamics on dynamically evolving networks can give new insight into the robustness of systems [38]; the dynamic system may be resilient to change in circumstances were an equivalent static time-averaged network would not.

This network sampling approach can, in principle, be adapted to the plant circadian network context. Indeed, we have shown in [15] that the DC2016 model is in fact a representation of a dynamic plant network governed by two different network structures depending on the phases of light and dark (rather than one static clock structure, as is usually depicted). Thus, the question that naturally arises is, is it possible to find underlying dynamic structures which potentially could explain the mechanisms of the plant clock to synchronize with the external environment? Answering this question might also help to explain the dynamical plasticity of the *Arabidopsis* clock [39]. A theoretical temporal approach could help to elucidate the temperature input pathway driving clock entrainment, and eventually to clarify the time scales governing the relationship between production and degradation of gene products which might explain the temperature compensation mechanism.

Appendix

Supplementary Material of this article is available online

References

[1] Schmelling NM, Axmann IM. Computational modelling unravels the precise clockwork of cyanobacteria. Interface Focus. 2018;8:20180038.

[2] Podkolodnaya OA, Tverdokhleb NN, Podkolodnyy NL. Computational modeling of the cell-autonomous mammalian circadian oscillator. BMC Systems Biology. 2017;11:27–42.

[3] Fathallah-Shaykh HM, Bona JL, Kadener S. Mathematical model of the Drosophila circadian clock: loop regulation and transcriptional integration. Biophysical journal. 2009;97:2399–408.

[4] Rand DA, Shulgin BV, Salazar D, Millar AJ. Design principles underlying circadian clocks. Journal of The Royal Society Interface. 2004;1:119–130.

[5] Rand DA, Shulgin B, Salazar D, Millar A. Uncovering the design principles of circadian clocks: Mathematical analysis of flexibility and evolutionary goals. Journal of Theoretical Biology. 2006;238:616–35.

[6] Locke JCW, Millar AJ, Turner MS. Modelling genetic networks with noisy and varied experimental data: the circadian clock in Arabidopsis thaliana. Journal of Theoretical Biology. 2005;234:383 – 393.

[7] Locke JCW, Southern MM, Kozma-Bognár L, Hibberd V, Brown PE, Turner MS, et al. Extension of a genetic network model by iterative experimentation and mathematical analysis. Molecular Systems Biology. 2005;1:0013.

[8] Locke JCW, Kozma-Bognár L, Gould PD, Fehér B, Kevei É, Nagy F, et al. Experimental validation of a predicted feedback loop in the multi-oscillator clock of Arabidopsis thaliana. Molecular Systems Biology. 2006;2:59.

[9] Pokhilko A, Hodge SK, Stratford K, Knox K, Edwards KD, Thomson AW, et al. Data assimilation constrains new connections and components in a complex, eukaryotic circadian clock model. Molecular Systems Biology. 2010;6:416.

[10] Pokhilko A, Fernández AP, Edwards KD, Southern MM, Halliday KJ, Millar AJ. The clock gene circuit in Arabidopsis includes a repressilator with additional feedback loops. Molecular Systems Biology. 2012;8:574.

[11] Pokhilko A, Mas P, Millar AJ. Modelling the widespread effects of TOC1 signalling on the plant circadian clock and its outputs. BMC Systems Biology. 2013;7:23.

[12] Fogelmark K, Troein C. Rethinking Transcriptional Activation in the Arabidopsis Circadian Clock. PLoS Computational Biology. 2014;10:e1003705.

[13] De Caluwé J, Xiao Q, Hermans C, Verbruggen N, Leloup JC, Gonze D. A Compact Model for the Complex Plant Circadian Clock. Frontiers in Plant Science. 2016;7:1–15.

[14] Bujdoso N, Davis SJ. Mathematical modeling of an oscillating gene circuit to unravel the circadian clock network of Arabidopsis thaliana. Frontiers in Plant Science. 2013;4:1–8.

[15] Avello PA, Davis SJ, Ronald J, Pitchford JW. Heat the Clock: Entrainment and Compensation in Arabidopsis Circadian Rhythms. Journal of Circadian Rhythms. 2019;17:5.

[16] Salomé PA, Weigel D, McClung CR. The role of the Arabidopsis morning loop components CCA1, LHY, PRR7, and PRR9 in temperature compensation. The Plant Cell. 2010;22:3650–61.

[17] Gould PD, Locke JCW, Larue C, Southern MM, Davis SJ, Hanano S, et al. The molecular basis of temperature compensation in the Arabidopsis circadian clock. The Plant Cell. 2006;18:1177–1187.

[18] Akman OE, Locke JCW, Tang S, Carré I, Millar AJ, Rand DA. Isoform switching facilitates period control in the Neurospora crassa circadian clock. Molecular Systems Biology. 2008;4:164.

[19] Hastings JW, Sweeney BM. On the Mechanism of Temperature Independence in a Biological Clock. Proceedings of the National Academy of Sciences of the United States of America. 1957;43:804–811.

[20] Ruoff P, Loros JJ, Dunlap JC. The relationship between FRQ-protein stability and temperature compensation in the Neurospora circadian clock. Proceedings of the National Academy of Sciences of the United States of America. 2005;102:17681–17686.

[21] Tsai TYC, Choi YS, Ma W, Pomerening JR, Tang C, Ferrell JE. Robust, Tunable Biological Oscillations from Interlinked Positive and Negative Feedback Loops. Science. 2008;321:126–129.

[22] Alon U. Network motifs: Theory and experimental approaches. Nature Reviews Genetics. 2007;8:450–461.

[23] Mangan S, Alon U. Structure and function of the feed-forward loop network motif. Proceedings of the National Academy of Sciences of the United States of America. 2003;100:11980–11985.

[24] Wong E, Baur B, Quader S, Huang CH. Biological network motif detection: principles and practice. Briefings in Bioinformatics. 2011 06;13:202–215.

[25] Alon U. An Introduction to Systems Biology: Design Principles of Biological Circuits. Taylor & Francis; 2006.

[26] Shen-Orr S, Milo R, Itzkovitz S, Kashtan N, Chklovskii S, Alon U. Network motifs in the transcriptional regulation network of Escherichia coli. Nature Genetics. 2002;31:64–68.

[27] Milo R, Shen-Orr S, Itzkovitz S, Kashtan N, Chklovskii D, Alon U. Network Motifs: Simple Building Blocks of Complex Networks. Science. 2002;298:824–827.

[28] Ignasius Joanito SHW Jhih-Wei Chu, Hsu CP. An incoherent feed-forward loop switches the Arabidopsis clock rapidly between two hysteretic states. Scientific Reports;8(13944).

[29] Adams S, Manfield I, Stockley P, Carré IA. Revised Morning Loops of the Arabidopsis Circadian Clock Based on Analyses of Direct Regulatory Interactions. PLOS ONE. 2015;10:1–11.

[30] Kamioka M, Takao S, Suzuki T, Taki K, Higashiyama T, Kinoshita T, et al. Direct Repression of Evening Genes by CIRCADIAN CLOCK-ASSOCIATED1 in the Arabidopsis Circadian Clock. The Plant Cell. 2016;28:696–711.

[31] Hsu CP, Lee PH, Chang CW, Lee CT. Constructing quantitative models from qualitative mutant phenotypes: preferences in selecting sensory organ precursors. Bioinformatics. 2006 03;22:1375–1382.

[32] Sidaway-Lee K, Costa MJ, Rand DA, Finkenstadt B, Penfield S. Direct measurement of transcription rates reveals multiple mechanisms for configuration of the Arabidopsis ambient temperature response. Genome Biology. 2014;15:R45.

[33] Ruoff P, Rensing L. The temperature-compensated Goodwin model simulates many circadian clock properties. Journal of Theoretical Biology. 1996;179:275–285.

[34] Farine DR, Whitehead H. Constructing, conducting and interpreting animal social network analysis. Journal of Animal Ecology. 2015;84:1144–1163.

[35] Pinter-Wollman N, Hobson EA, Smith JE, Edelman AJ, Shizuka D, de Silva S, et al. The dynamics of animal social networks: analytical, conceptual, and theoretical advances. Behavioral Ecology. 2013;25:242–255.

[36] Blonder B, Wey TW, Dornhaus A, James R, Sih A. Temporal dynamics and network analysis. Methods in Ecology and Evolution. 2012;3:958–972.

[37] Blonder B, Dornhaus A. Time-Ordered Networks Reveal Limitations to Information Flow in Ant Colonies. PLOS ONE. 2011;6:1–8.

[38] Burns D, Pitchford JW, Parr CL, Franks DW, Robinson EJH. The costs and benefits of decentralization and centralization of ant colonies. Behavioral Ecology. 2019;30:1700–1706.

[39] Webb AAR, Seki M, Satake A, Caldana C. Continuous dynamic adjustment of the plant circadian oscillator. Nature Communications. 2019;10:550.

Supplementary Material

Transcription matrices

L2005a →

	CL	TOC1
CL		−
TOC1	+	

L2005b →

	CL	TOC1	X	Y
CL		−		−
TOC1			+	−
X	+			
Y		+		

L2006 →

	CL	TOC1	X	Y	PRR9/7
CL		−		−	+
TOC1			+	−	
X	+				
Y		+			
PRR9/7	−				

P2010 →

	CL	TOC1	Y	PRR9	PRR7	PRR5
CL		−	−	+	+	+
TOC1	+		−	−		
Y		+				
PRR9	−				+	
PRR7	−					+
PRR5	−					

P2012 →

	CL	PRR9	PRR7	PRR5	TOC1	ELF4	ELF3	LUX
CL		+	+	+	−	−	−	−
PRR9	−		+					
PRR7	−			+				
PRR5	−							
TOC1	−							
E34L		−			−	−		−

P2013 →

	CL	PRR9	PRR7	PRR5	TOC1	ELF4	ELF3	LUX
CL		+	+	+	−	−	−	−
PRR9	−		+					
PRR7	−			+				
PRR5	−							
TOC1	−	−	−	−		−		−
E34L		−			−	−		−

$$\mathbf{F2014} \rightarrow$$

	$CCA1$	LHY	$PRR9$	$PRR7$	$PRR5$	$TOC1$	$ELF4$	$ELF3$	LUX	$RVE8$
$CCA1$		−	−	−	−	−	−	−	−	
LHY		−	−	−	−	−	−	−	−	
$PRR9$	−	−								−
$PRR7$	−	−								−
$PRR5$	−	−	−	−						−
$TOC1$	−	−	−	−	−	−	−		−	
$E34L$		−	−	−	−	−			−	
$RVE8$			+		+	+	+		+	

$$\mathbf{DC2016} \rightarrow$$

	CL	$P97$	$P51$	EL
CL		+	−	−
$P97$	−			
$P51$	−	−	−	−
EL	−			−

Table S1

Parameters of the models affected by temperature.

ODE model	Rate constants of translation
L2005a	p_1, p_2
L2005b	p_1, p_2, p_3, p_4
L2006	p_1, p_2, p_3, p_4, p_6
P2010	p_1, p_2, p_4, p_6, p_8, p_9, p_{10}
P2012	p_1, p_2, p_4, p_8, p_9, p_{10}, p_{23}, p_{27}
P2013	p_1, p_2, p_4, p_8, p_9, p_{10}, p_{23}, p_{27}
F2014	p_1, p_2, p_3, p_4, p_5, p_{16}, p_{23}, p_{30}, p_{31}, p_{32}
DC2016	p_1, p_{1L}, p_2, p_3, p_4

Minimal models

The S1 model

$$\frac{d[CL]_m}{dt} = \beta_1 * \frac{1}{1 + (\frac{[P97]_p}{K_1})^n + (\frac{[P51]_p}{K_2})^n} - d_1 * [CL]_m$$

$$\frac{d[CL]_p}{dt} = p_1 * [CL]_m - d_2 * [CL]_p$$

$$\frac{d[P97]_m}{dt} = \beta_2 * \frac{1}{1 + (\frac{[CL]_p}{K_3})^n + (\frac{[EL]_p}{K_4})^n} - d_3 * [P97]_m$$

$$\frac{d[P97]_p}{dt} = p_2 * [P97]_m - d_4 * [P97]_p$$

$$\frac{d[P51]_m}{dt} = \beta_3 * \frac{1}{1 + (\frac{[CL]_p}{K_5})^n} - d_5 * [P51]_m$$

$$\frac{d[P51]_p}{dt} = p_3 * [P51]_m - d_6 * [P51]_p$$

$$\frac{d[EL]_m}{dt} = \beta_4 * \frac{1}{1 + (\frac{[CL]_p}{K_6})^n} - d_7 * [EL]_m$$

$$\frac{d[EL]_p}{dt} = p_4 * [EL]_m - d_8 * [EL]_p$$

The S2 model

$$\frac{d[CL]_m}{dt} = \beta_1 * \frac{1}{1 + (\frac{[P97]_p}{K_1})^n + (\frac{[P51]_p}{K_2})^n} - d_1 * [CL]_m$$

$$\frac{d[CL]_p}{dt} = p_1 * [CL]_m - d_2 * [CL]_p$$

$$\frac{d[P97]_m}{dt} = \beta_2 * \frac{1}{1 + (\frac{[CL]_p}{K_3})^n + (\frac{[EL]_p}{K_4})^n} - d_3 * [P97]_m$$

$$\frac{d[P97]_p}{dt} = p_2 * [P97]_m - d_4 * [P97]_p$$

$$\frac{d[P51]_m}{dt} = \beta_3 * \frac{1}{1 + (\frac{[CL]_p}{K_5})^n + (\frac{[P51]_p}{K_7})^n} - d_5 * [P51]_m$$

$$\frac{d[P51]_p}{dt} = p_3 * [P51]_m - d_6 * [P51]_p$$

$$\frac{d[EL]_m}{dt} = \beta_4 * \frac{1}{1 + (\frac{[CL]_p}{K_6})^n + (\frac{[EL]_p}{K_8})^n} - d_7 * [EL]_m$$

$$\frac{d[EL]_p}{dt} = p_4 * [EL]_m - d_8 * [EL]_p$$

Table S2
Selecting parameter sets for the clock structures in Figure 4. Percentages in brackets were calculated over the number of parameter sets searched (third column). Last column shows the number of sets including the parameters to be applied Arrhenius equations.

Models	number of parameters	sets searched	sets oscillating	oscillating and phase
S1	23	500,000	2,114 (0.42%)	1,281 (0.26%)
S2	25	500,000	1,870 (0.37%)	239 (0.05%)
S3	26	500,000	1,880 (0.38%)	137 (0.03%)

The S3 model

$$\frac{d[CL]_m}{dt} = \beta_1 * \frac{1}{1 + (\frac{[P97]_p}{K_1})^n + (\frac{[P51]_p}{K_2})^n} - d_1 * [CL]_m$$

$$\frac{d[CL]_p}{dt} = p_1 * [CL]_m - d_2 * [CL]_p$$

$$\frac{d[P97]_m}{dt} = \beta_2 * \frac{1}{1 + (\frac{[CL]_p}{K_3})^n + (\frac{[EL]_p}{K_4})^n} - d_3 * [P97]_m$$

$$\frac{d[P97]_p}{dt} = p_2 * [P97]_m - d_4 * [P97]_p$$

$$\frac{d[P51]_m}{dt} = \beta_3 * \frac{1}{1 + (\frac{[CL]_p}{K_5})^n + (\frac{[P51]_p}{K_7})^n} - d_5 * [P51]_m$$

$$\frac{d[P51]_p}{dt} = p_3 * [P51]_m - d_6 * [P51]_p$$

$$\frac{d[EL]_m}{dt} = \beta_4 * \frac{1}{1 + (\frac{[CL]_p}{K_6})^n + (\frac{[EL]_p}{K_8})^n + (\frac{[P51]_p}{K_9})^n} - d_7 * [EL]_m$$

$$\frac{d[EL]_p}{dt} = p_4 * [EL]_m - d_8 * [EL]_p$$
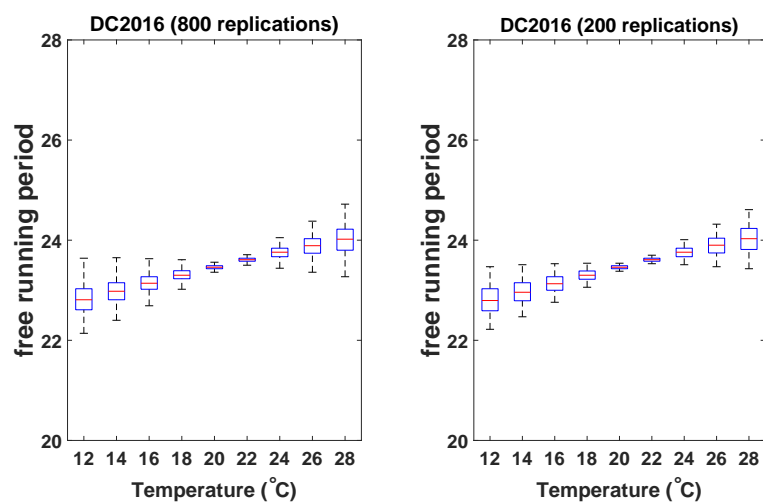
Figure S1: Modelled outputs do not change when a small number of replications is used. Modelled outcomes from DC2016 model for different number of replications. Simulations were carried out following experimental protocols of [16] and [17]. Results show the distribution of the free-running period when random uniformly distributed activation energy values between 40 kJmol^{-1} and 60 kJmol^{-1} were allocated independently to the translation rates of the model.
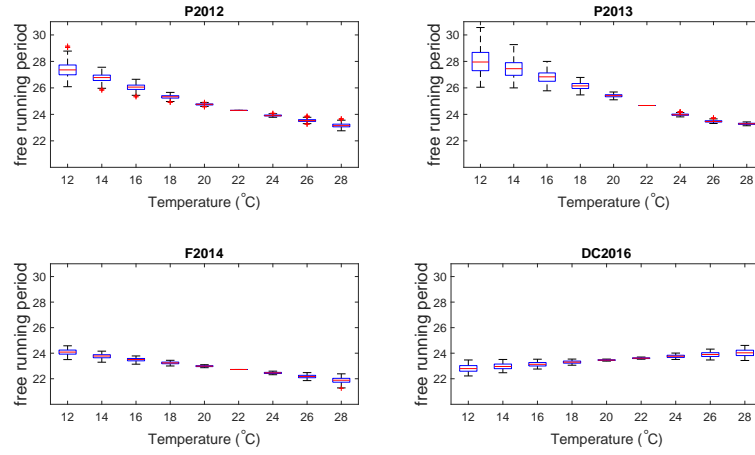
Figure S2: The models P2012, P2013, F2014 and DC2016 exhibit temperature compensation. Simulations were carried out following experimental protocols of [16] and [17]. Results show the distribution of the free-running period when random uniformly distributed activation energy values between 40 kJmol^{-1} and 60 kJmol^{-1} were allocated independently to the translation rates of the model. Results support outputs obtained in Figure 5, where the influence of temperature was parametrized to be equal.
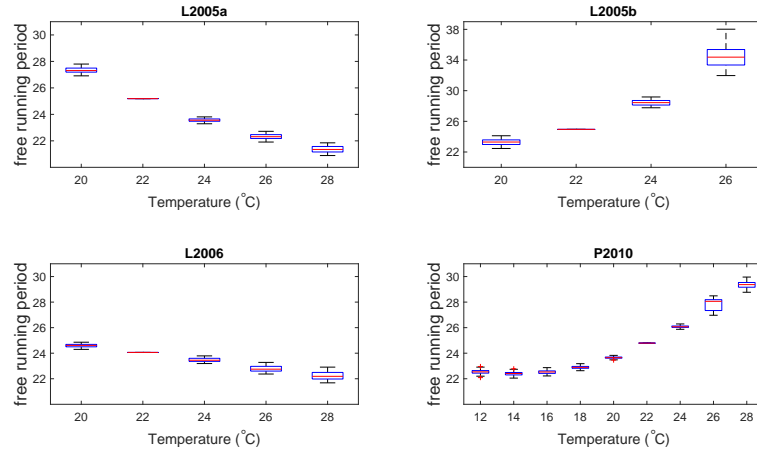
Figure S3: The earliest clock models, L2005a, L2005b, L2006 and P2010 do not exhibit temperature compensation. Simulations were carried out following experimental protocols of [16] and [17]. Results show the distribution of the free-running period when random uniformly distributed activation energy values between 40 kJmol^{-1} and 60 kJmol^{-1} were allocated independently to the translation rates of the model. Results support outputs obtained in Figure 5, where the influence of temperature was parametrized to be equal.
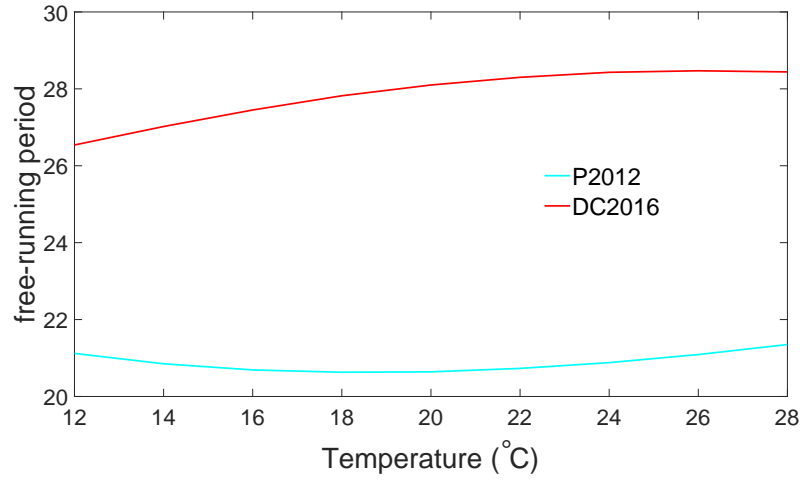
Figure S4: Autoregulation alone is inadequate to explain temperature compensation. The figure shows outputs from modified P2012 and DC2016 models, where the autoregulation loops have been removed. In both cases, temperature compensation persists in spite of the change to the network structure.
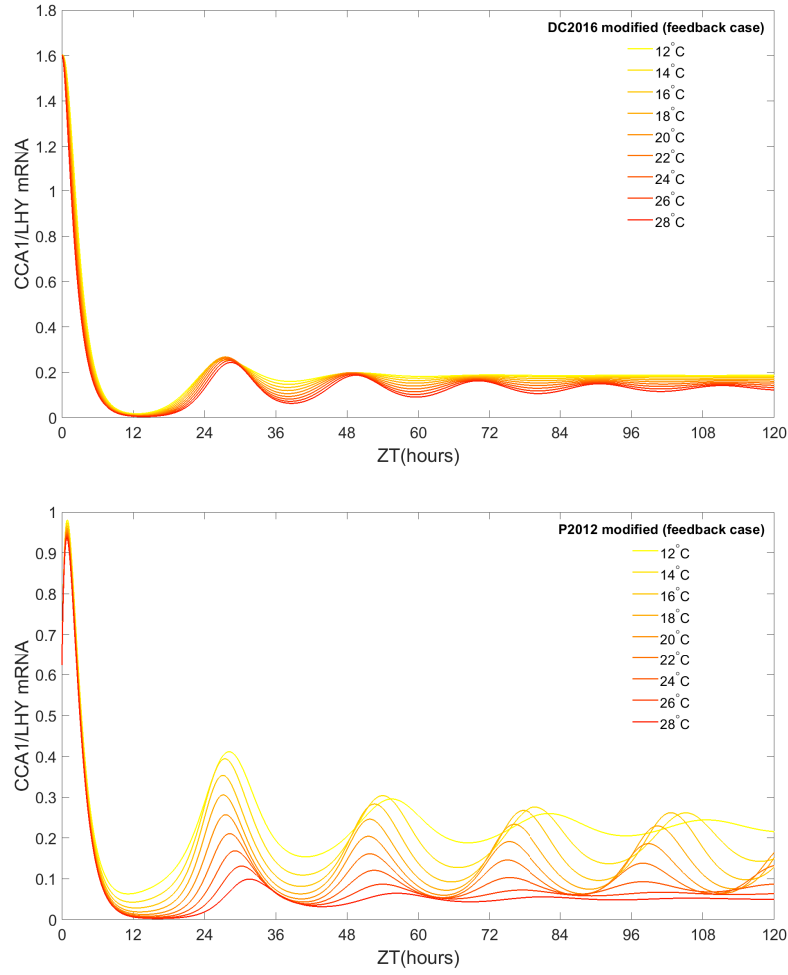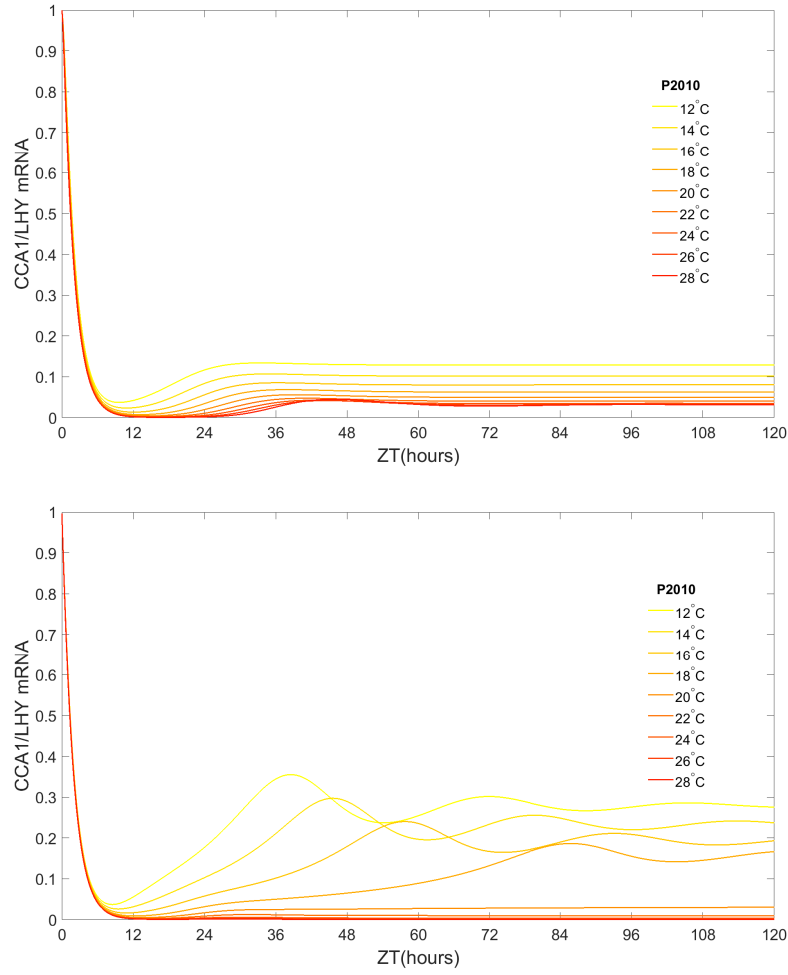
Figure S5: Simulated *CCA1/LHY* expression under constant light for a disrupted three-node feedback. Upper figure: DC2016 model with loss of interaction of *ELF4/LUX* on *PPR9/PRR7*. Lower figure: P2012 model with loss of interaction of *ELF4/LUX* on *PRR9*.
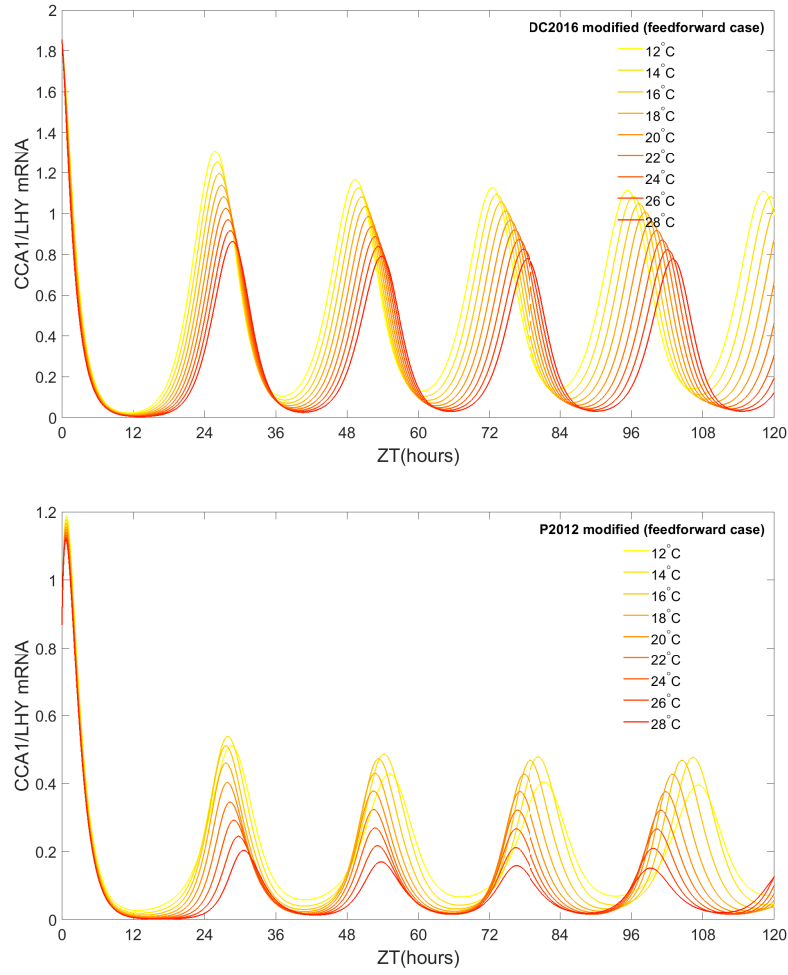
Figure S6: Simulated *CCA1/LHY* expression under constant light for a disrupted feedforward. Upper figure: DC2016 model with loss of interaction of *PRR5/TOC1* on *ELF4/LUX*. Lower figure: P2012 model with loss of interaction of *CCA1/LHY* on *TOC1*.
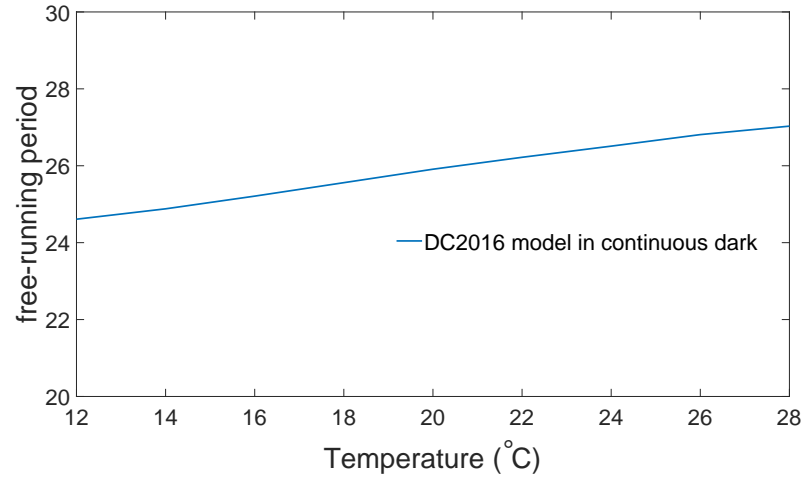
Figure S7: Temperature compensation persists under continuous dark conditions but with a reduced Q_{10} of period compared to constant light. The figure shows outputs from DC2016 model, where *ELF4/LUX* autoregulation with a three-node feedback loops are absent due to dark phase. A Q_{10} equal to 0.94 is observed.

Figure S8: Simulated *CCA1/LHY* expression under constant light for different temperatures. Upper figure: Outputs from P2010 model, where positive interactions on *CCA1/LHY*, *TOC1*, *PRR5*, *PRR9* and *PRR7* are removed. Lower figure: Outputs from P2010 model, where positive interactions on *CCA1/LHY*, *TOC1* and *PRR9* are changed to negative.
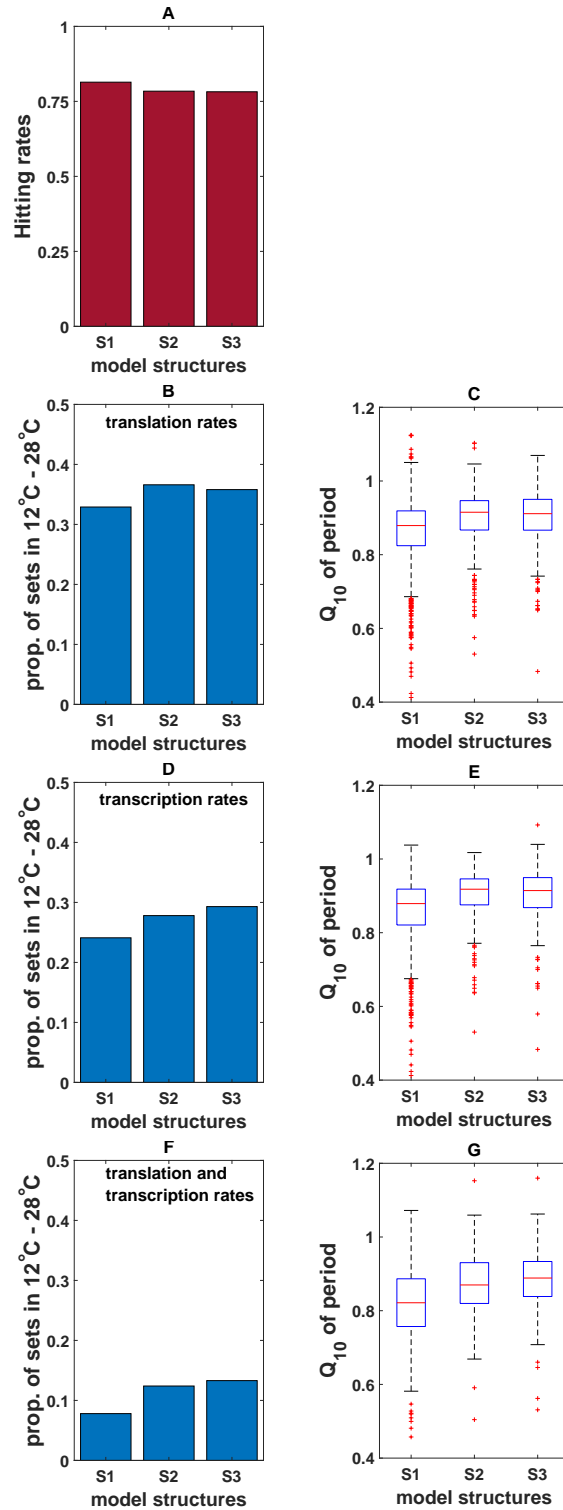
Figure S9: Autoregulation together with three-node feedback structure improves the robustness of the system against temperature changes. Results from random parameterisations of models S1, S2 and S3 in Figure 4 when modelled inputs were chosen from uniform distributed numbers with mean equal to the published parameter values for DC2016 model rather than from uniform distributed numbers between 0 and 1 as shown in Figure 6. (A) Normalized proportion of parameter sets that showed sustained oscillations and correct order of peak gene expression. (B, D, F) Proportion of parameter sets that allowed the system to oscillate across a 12°C - 28°C temperature range with respect to the number of sets obtained after searching (see Tables S6 to S8 in Supplementary Material for absolute frequencies). Note that the ranking of models S1-S3 is unchanged from that in Figure 6, but that the relative differences are very much diminished. (C, E, G) Distribution of the modelled outputs of the parameter sets selected to show oscillatory behaviour in the range 12°C - 28°C.

Table S3

Parameter sets producing sustained oscillations on a range of 12°C to 28°C in temperature-dependent translation rates. Parameterisations from uniformly distributed numbers between 0 and 1. Third column shows the number of modelled inputs for Figure 6C.

Models	sets selected	sets in [12°C ; 28°C]	% obtained
S1	1,281	188	14.7
S2	239	72	30.1
S3	137	38	27.7

Table S4

Parameter sets producing sustained oscillations on a range of 12°C to 28°C in temperature-dependent transcription rates. Parameterisations from uniformly distributed numbers between 0 and 1. Third column shows the number of modelled inputs for Figure 6E.

Models	sets selected	sets in [12°C ; 28°C]	% obtained
S1	1,281	123	9.6
S2	239	52	21.8
S3	137	32	23.4

Table S5

Parameter sets producing sustained oscillations on a range of 12°C to 28°C in temperature dependent translation and transcription rates. Parameterisations from uniformly distributed numbers between 0 and 1. Third column shows the number of modelled inputs for Figure 6G.

Models	sets selected	sets in [12°C ; 28°C]	% obtained
S1	1,281	10	0.8
S2	239	9	3.8
S3	137	6	4.4

Table S6
Parameter sets producing sustained oscillations on a range of 12°C to 28°C in temperature-dependent translation rates. Parameterisations from uniformly distributed numbers between zero and two-fold the value of the relevant parameters published in DC2016. Third column shows the number of modelled inputs for Figure S9C.

Models	sets selected	sets in [12°C ; 28°C]	% obtained
S1	4,403	1,450	32.9
S2	1,141	418	36.6
S3	836	299	35.8

Table S7
Parameter sets producing sustained oscillations on a range of 12°C to 28°C in temperature-dependent transcription rates. Parameterisations from uniformly distributed numbers between zero and two-fold the value of the relevant parameters published in DC2016. Third column shows the number of modelled inputs for Figure S9E.

| Models	sets selected	sets in [12°C ; 28°C]	% obtained
S1	4,403	1,059	24.1
S2	1,141	317	27.8
S3	836	245	29.3

Table S8
Parameter sets producing sustained oscillations on a range of 12°C to 28°C in temperature dependent translation and transcription rates. Parameterisations from uniformly distributed numbers between zero and two-fold the value of the relevant parameters published in DC2016. Third column shows the number of modelled inputs for Figure S9G.

| Models	sets selected	sets in [12°C ; 28°C]	% obtained
S1	4,403	343	7.8
S2	1,141	142	12.4
S3	836	111	13.3
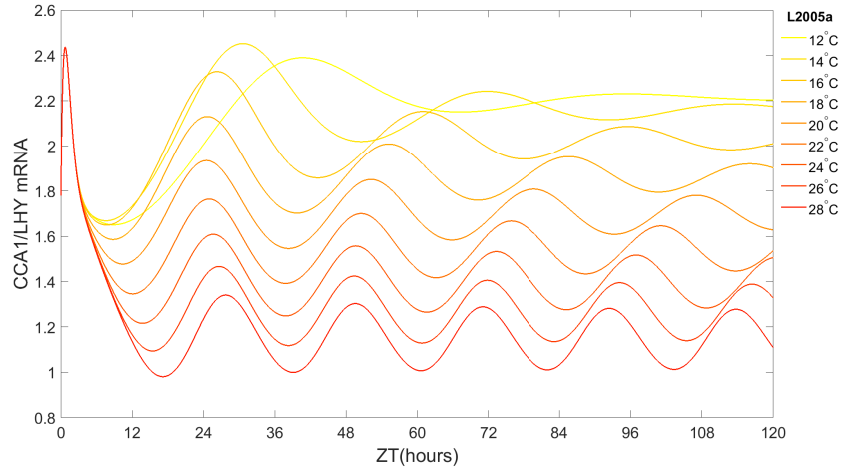
Figure S10: Temperature dependence in L2005a model. Modelled outcomes from L2005a model for an activation energy value of 50 kJmol^{-1}. Simulations were carried out following experimental protocols of [16] and [17]. Results show mRNA levels of *CCA1/LHY* under free-running conditions for a range of temperatures.
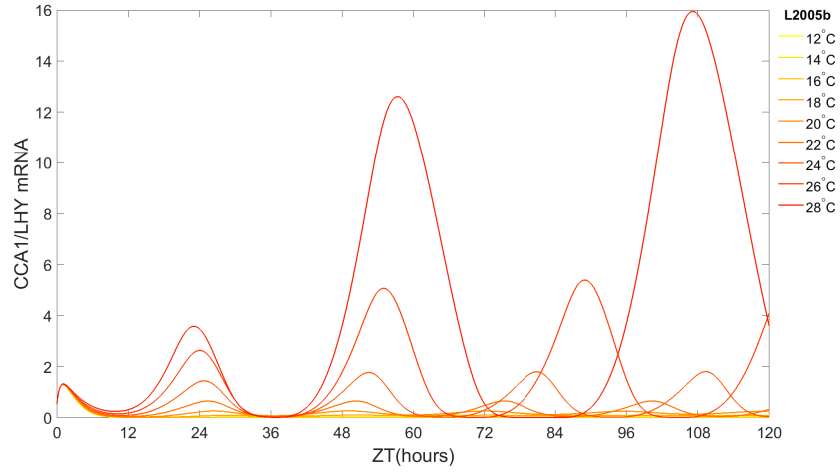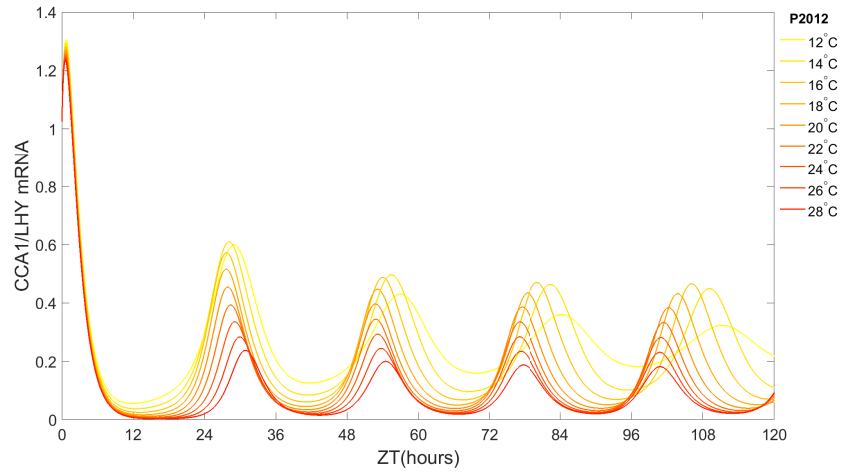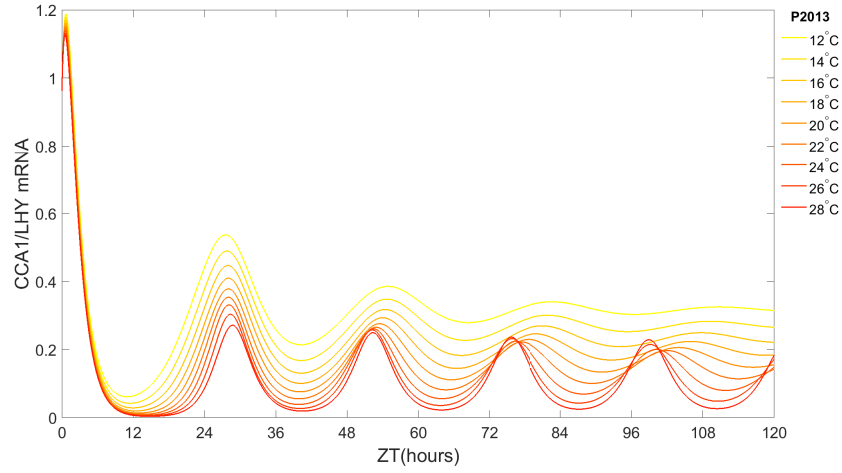
Figure S11: Temperature dependence in L2005b model. Modelled outcomes from L2005b model for an activation energy value of 50 kJmol^{-1}. Simulations were carried out following experimental protocols of [16] and [17]. Results show mRNA levels of *CCA1/LHY* under free-running conditions for a range of temperatures.
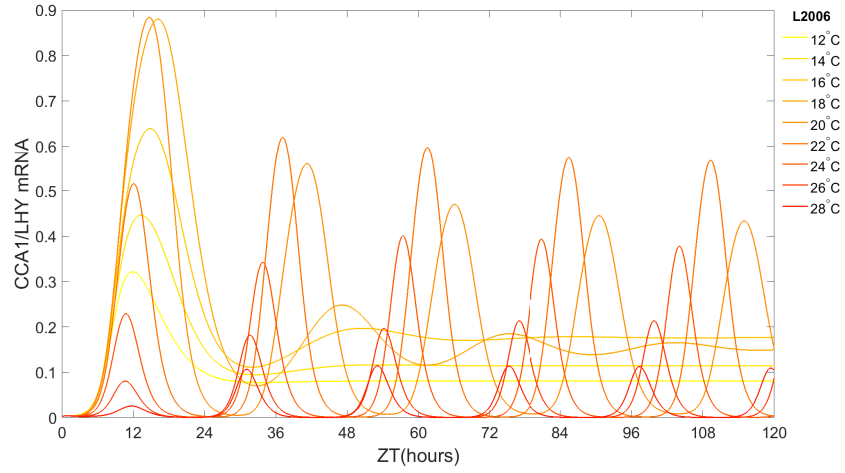
Figure S12: Temperature dependence in L2006 model. Modelled outcomes from L2006 model for an activation energy value of 50 kJmol^{-1}. Simulations were carried out following experimental protocols of [16] and [17]. Results show mRNA levels of *CCA1/LHY* under free-running conditions for a range of temperatures.
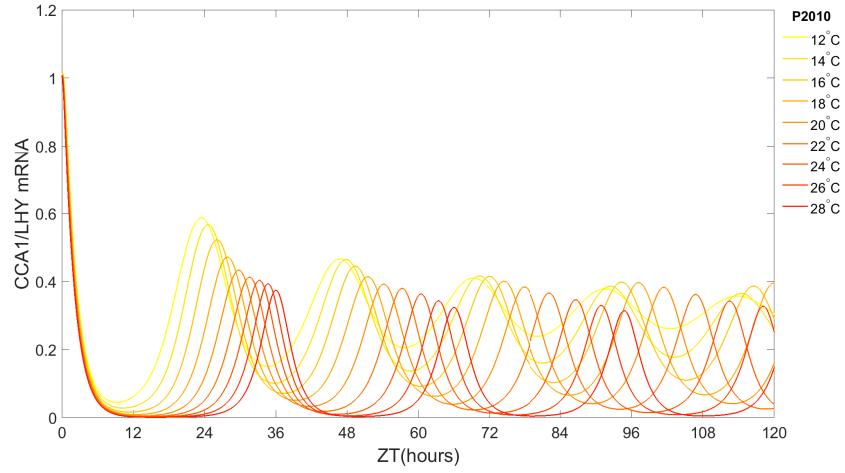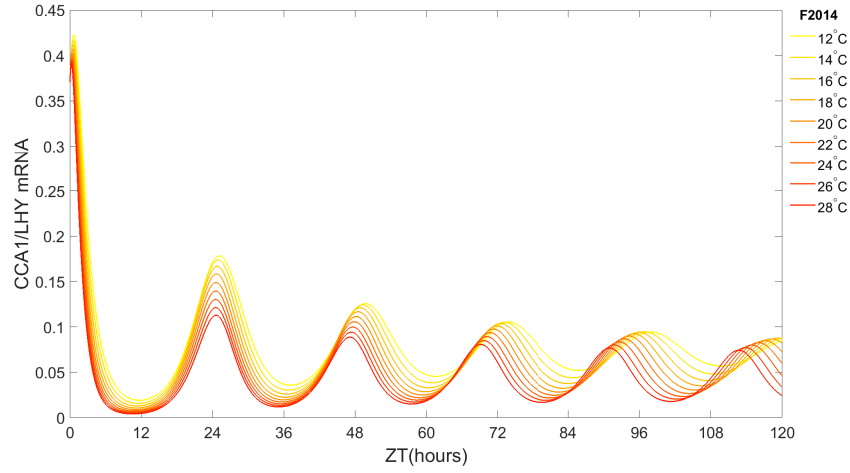
Figure S13: Temperature dependence in P2010 model. Modelled outcomes from P2010 model for an activation energy value of 50 kJmol^{-1}. Simulations were carried out following experimental protocols of [16] and [17]. Results show mRNA levels of *CCA1/LHY* under free-running conditions for a range of temperatures.
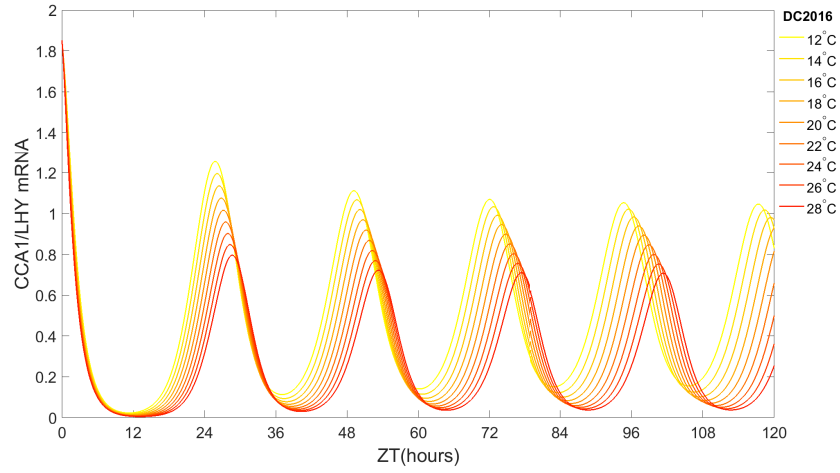
Figure S14: Temperature dependence in P2012 model. Modelled outcomes from P2012 model for an activation energy value of 50 kJmol^{-1}. Simulations were carried out following experimental protocols of [16] and [17]. Results show mRNA levels of *CCA1/LHY* under free-running conditions for a range of temperatures.

Figure S15: Temperature dependence in P2013 model. Modelled outcomes from P2013 model for an activation energy value of 50 kJmol^{-1}. Simulations were carried out following experimental protocols of [16] and [17]. Results show mRNA levels of *CCA1/LHY* under free-running conditions for a range of temperatures.

Figure S16: Temperature dependence in F2014 model. Modelled outcomes from F2014 model for an activation energy value of 50 kJmol^{-1}. Simulations were carried out following experimental protocols of [16] and [17]. Results show mRNA levels of *CCA1/LHY* under free-running conditions for a range of temperatures.

Figure S17: Temperature dependence in DC2016 model. Modelled outcomes from DC2016 model for an activation energy value of 50 kJmol^{-1}. Simulations were carried out following experimental protocols of [16] and [17]. Results show mRNA levels of *CCA1/LHY* under free-running conditions for a range of temperatures.